HHS Public Access

Author manuscript

Biochem Pharmacol. Author manuscript; available in PMC 2016 November 01.

Published in final edited form as:

Biochem Pharmacol. 2014 May 1; 89(1): 131–140. doi:10.1016/j.bcp.2014.02.002.

Presence of multiple binding sites on α9α10 nAChR receptors alludes to stoichiometric dependent action of the α-conotoxin, Vc1.1

Dinesh C. Indurthi[1], **Elena Pera**[1], **Hye-Lim Kim**[1], **Cindy Chu**[1], **Malcolm D. McLeod**[2], **J. Michael McIntosh**[3], **Nathan L. Absalom**[*,1], and **Mary Chebib**[*,1]

[1]Faculty of Pharmacy, University of Sydney, NSW, 2006, Australia.

[2]Research School of Chemistry, Australian National University, Canberra, ACT, 0200, Australia

[3]George E. Wahlen Veterans Affairs Medical Center, Salt Lake City, Utah 84108, and Departments of Psychiatry and Biology, University of Utah, Salt Lake City, UT 84112, USA.

Abstract

Nicotinic acetylcholine receptors (nAChRs) are ligand-gated ion channels involved in fast synaptic transmission. nAChRs are pentameric receptors formed from a combination of different or similar subunits to produce heteromeric or homomeric channels. The heteromeric, α9α10 nAChR subtype is well-known for its role in the auditory system, being expressed in cochlear hair cells. These nAChRs have also been shown to be involved in immune-modulation. Antagonists of α9α10 nAChRs, like the α-conotoxin Vc1.1, have analgesic effects in neuropathic pain. Unlike other nAChR subtypes there is no evidence that functional receptor stoichiometries of α9α10 exist. By using 2-electrode voltage clamp methods and maintaining a constant intracellular Ca^{2+} concentration, we observed a biphasic activation curve for ACh that is dependent on receptor stoichiometry. Vc1.1, but not the α9α10 antagonists RgIA or atropine, inhibits ACh-evoked currents in a biphasic manner. Characteristics of the ACh and Vc1.1 activation and inhibition curves can be altered by varying the ratio of α9 and α10 mRNA injected into oocytes, changing the curves from biphasic to monophasic when an excess of α10 mRNA is used. These results highlight the difference in the pharmacological profiles of at least two different α9α10 nAChR stoichiometries, possibly $(\alpha9)_3(\alpha10)_2$ and $(\alpha9)_2(\alpha10)_3$. As a result, we infer that there is an additional binding site for ACh and Vc1.1 at the α9-α9 interface on the hypothesized $(\alpha9)_3(\alpha10)_2$ nAChR, in addition to the α10-α9 and or α9-α10 interfaces that are common to both stoichiometries. This study provides further evidence that receptor stoichiometry contributes another layer of complexity in understanding Cys-loop receptors.

[*]**Corresponding Authors:** Mary Chebib, Faculty of Pharmacy, A15, University of Sydney, NSW, 2006, Australia, +61293518584, +61293514391, mary.collins@sydney.edu.au, Nathan L. Absalom, Faculty of Pharmacy, A15, University of Sydney, NSW, 2006, Australia, +61293516066, +61293514391, nathan.absalom@sydney.edu.au.

Conflicts of Interest

The authors have no conflicts of interest

Graphical Abstract

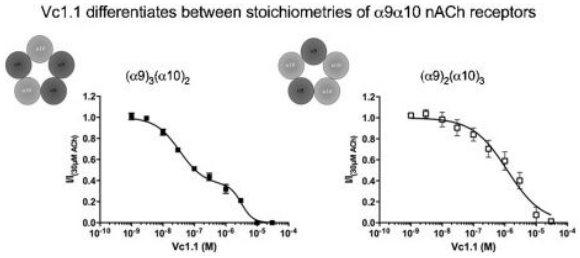

Keywords

Nicotinic acetylcholine receptors; subunit stoichiometry; α-conotoxins; Vc1.1; RgIA; alpha9alpha10

1.0 Introduction

Nicotinic acetylcholine receptors (nAChRs) are members of the ligand-gated ion channel (LGIC) superfamily that mediate fast synaptic transmission between cells of both the central and peripheral nervous systems [1]. Receptors are formed by a pentameric arrangement of subunits that surround a central ion-conducting pore [1]. To date, 14 nACh subunits (α1-α10, β1-4) have been cloned from vertebrates [2]. Each subunit contains a large extracellular domain, four transmembrane regions (M1-M4), of which the second M2 contains the amino acids that line the channel pore, two short transmembrane loops (M1-M2, M3-M4) that act as “hinges” for channel gating, and a large intracellular loop (M3-M4) that controls ion conductivity and interacts with scaffolding proteins [3]. The ACh-binding site is located at the interface of subunits in the extracellular domain, approximately 30 Å away from the gating region of the pore where cations passively cross the membrane [4].

The α9 and α10 subunits are known to form a heteromeric receptor in the mammalian cochlea and mediate postsynaptic transmission between the olivocochlear fibres and the outer hair cells [5]. Initial studies were not able to detect currents recorded from hair cells that express only α9 subunits [6] yet subsequent studies demonstrated that currents of diminished amplitude could be recorded from outer hair cells in α10 null-mutant mice [7]. This indicates α9 homomeric receptors do form functional receptors but the currents observed from these channels are very small and that the most likely physiologically relevant receptor in this tissue are α9α10 heteromeric receptors. α9α10 nAChRs are thought to be involved in the molecular mechanisms attributing protection of the inner ear from excess sound [8].

The α9 and α10 subunits have also been identified in lymphocytes, skin keratinocytes, sperm and dorsal root ganglion (DRG) [9-13]. Although the role of α9α10 nAChRs at a molecular level in non-auditory systems are not well understood, α-conotoxin (α-CTx) antagonists of α9α10 such as Vc1.1, a cysteine-rich peptide isolated from *Conus victoriae* [14] and RglA isolated from the marine snail *Conus regius* [15] display analgesic properties in rat models of neuropathic pain, possibly via immunomodulatory effect [16]. Blockade of

this nAChR subtype was shown to reduce the number of choline acetyltransferase-positive cells (macrophages and lymphocytes) at the site of injury [16].

Although these toxins display a high degree of selectivity for the α9α10 receptor over other nAChR subtypes [16], the exact mechanism of action for alleviating pain is not really known and other target sites have been proposed including inhibiting the N-type Ca^{2+} channels in an indirect manner. In rodent DRG neurons, Vc1.1 and RglA were shown to inhibit Voltage Gated Calcium Channel via activating $GABA_B$ receptors [17-19], in a mechanism that is independent of α9α10 nAChRs [20].

The stoichiometry of α9α10 was initially suggested to be $(α9)_2(α10)_3$ in oocytes [21]. Using this stoichiometry, molecular modeling and docking studies showed that ACh and the α-CTx RglA bind to the principal α9 (+) side (α9-α10) and complementary α10 (−) side of the α9α10 binding pocket [22]. However, mutational studies aimed at understanding the differential sensitivity of rat and human α9α10 nAChR to α-CTx RglA, revealed an interaction of this α-CTx at the complementary (−) side of α9 and the principal (+) side of α10 (α10-α9 binding interface) [23]. Likewise Vc1.1 binds to the α10-α9 binding interface as evidenced by comparing calculated mutational energies to that observed from electrophysiological recordings [24].

In this study, we demonstrate the existence of a novel binding site for Vc1.1 on α9α10 nAChRs by investigating the pharmacology of Vc1.1 inhibition of α9α10 nAChRs with and without Ca^{2+}. We also investigated whether Vc1.1 inhibits α9 receptors with a different sensitivity, or whether α9α10 nAChRs exist in different stoichiometries that differ in sensitivity to Vc1.1. We also determined whether RgIA [15] or the small molecule, atropine [25, 26], two other known α9α10 antagonists can also discriminate between different stoichiometries of α9α10 nAChRs. We found that by eliminating Ca^{2+} from the extracellular solution, and then buffering intracellular Ca^{2+}, Vc1.1 but not RgIA or atropine inhibits α9α10 receptors in a biphasic manner. We demonstrated that Vc1.1 inhibition of α9 homomeric receptors is unlikely to explain this biphasic phenomenon. Using altered ratios of α9 and α10 mRNA injection ratio, we demonstrated that Vc1.1 binds to at least one binding site that is common to the various α9α10 stoichiometries, but also binds to an additional binding site located at an α9-α9 interface in stoichiometries that contain more α9 than α10 subunits.

2.0 Materials and Methods

2.1 Reagents

HEPES (hemisodium salt), sodium pyruvate, theophylline, ethylene glycol tetraacetic acid (EGTA), atropine, naringin, lysophosphatidic acid, tricaine, gentamycin, kanamycin and 1,2-**b**is(O-**a**mino**p**henoxy)ethane-N,N,N',N'-**t**etra**a**cetic acid (BAPTA) from Sigma, Castle Hill, NSW, Australia.

2.2 Expression of recombinant α9 and α10 receptors in Xenopus oocytes

Rat α9 and α10 cDNAs subcloned in a modified pGEMHE vector [27] were kind gifts from Dr. A.B. Elgoyhen (Universidad de Buenos Aires, Buenos Aires, Argentina). Rat α9 and

α10 plasmids were linearized using *Nhe*I (New England Biolabs, Ipswich, MA, USA). mRNAs were transcribed *in vitro* using T7 mMessage mMachine™ (Ambion Inc., Austin, TX, USA) transcription kit. Where indicated, plasmids were linearised with *Hind*III and the transcribed mRNA was polyadenylated using the poly-A-tailing kit (Ambion Inc., Austin, TX, USA). RNAs were purified with the MEGAClear RNA purification kit (Ambion Inc., Austin, TX, USA) or lithium chloride precipitation. RNA was treated with DNase prior to purification and RNA concentrations were measured by spectrophotometry using the Nanodrop (Thermal Fisher Scientific). The RNA was then diluted in ratios of α9:α10 10:1, 1:1, 1:3 and 1:10. RNA was injected at a ratio of 1:1 unless otherwise stated in the text.

2.3 Xenopus laevis surgery, oocyte extraction and injection

The experiments were performed with Animal Ethics approvals from The University of Sydney (ethics approval number K21/1-2013/3/5915). Female *X. laevis* was anesthetized with tricaine (850mg/500mL). Several ovarian lobes were surgically removed by a small incision on the abdomen of the *X. laevis*. The *X. laevis* were allowed to recover from the surgery the time interval between surgical procedures on each frog was 6-12 months. Five recoverable surgeries were performed on each *X. laevis* and a final terminal surgery, with the frog exposed to a lethal dose of anaesthetic. The lobes were cut into small pieces and were rinsed thoroughly with oocyte releasing buffer 2 (OR2; 82.5mM NaCl, 2mM KCl, 1mM $MgCl_2$, 5mM HEPES (hemi-Na)). The lobes were digested with collagenase A (2mg/mL in OR2; Boehringer Manheim, Germany) at room temperature. The oocytes were further washed with OR2 and stored in Frog Ringer buffer (ND96) wash solution (96mM NaCl, 2mM KCl, 1mM $MgCl_2$, 1.8mM $CaCl_2$, 5mM HEPES (hemisodium salt), supplemented with 2.5mM sodium pyruvate and 0.5mM theophylline, until ready for injection. Stage V–VI oocytes were selected and microinjected with 2ng mRNA in 50.6nL H_2O. After injection, the oocytes were maintained at 18°C in the presence of ND96 wash solution augmented with 50μg/mL kanamycin.

2.4 Electrophysiological recording of recombinant receptors

Whole-cell currents were measured using a two-electrode voltage clamp with a Digidata 1200, Geneclamp 500B amplifier together with a Powerlab/200 (AD Instruments, Sydney, Australia) and Chart version 3.5 for PC as previously described. The recording microelectrodes were filled with 3 M KCl and had resistance between 0.2 and 1 MΩ. Where indicated, intracellular Ca^{2+} was buffered with 11mM EGTA added to the solution in the recording microelectrode and was allowed to equilibrate in the oocyte for 15 minutes prior to recording. Three to 7 days post-injection, oocytes held at −60 mV were used for recording. While recording, oocytes were superfused with Frog Ringer (ND96) until a stable base current was reached. Increasing concentrations of Vc1.1 (Tocris Bioscience, Bristol, UK), RgIA (synthesized as described previously [15] or atropine was evaluated in the absence and presence of a submaximal concentration of ACh (30 μM), respectively, until maximal current was reached, at which time the oocyte was washed for 12 min to allow complete recovery of response to acetylcholine (30 μM). Unless otherwise indicated, Ca^{2+} free, 1.8mM Ba^{2+} solution was used that contained 115mM NaCl, 2.5mM KCl, 1.8mM $BaCl_2$, 10mM HEPES and “low divalent” buffer contained 115mM NaCl, 2.5mM KCl, 0.2mM $CaCl_2$, 10mM HEPES. Where indicated a stock concentration of 5mg/mL 1,2-bis

(O-aminophenoxy)ethane-N,N,N',N'-tetracetic acid (BAPTA) was dissolved into 0.3N Na_2CO_3 and then pH adjusted to 7 and 50.6nL injected to oocytes immediately prior to recording.

2.5 Data analysis

The amplitude of each current response to ACh (I) was normalized to the amplitude of the maximum current response to ACh (I_{max}) according to the following equation:

$$\text{Normalized Response} = I/I_{max}$$

Normalized concentration-response curves were constructed and analyzed using GraphPad "Prism" version 5.0 according to the equation:

$$I = I_{max}\left([\mathrm{A}]^{n_\mathrm{H}} / \left([\mathrm{A}]^{n_\mathrm{H}} + EC_{50}{}^{n_\mathrm{H}}\right)\right)$$

Where [A] is the ligand concentration and n_H is the Hill slope. Mean parameters of each curve were derived from at least three oocytes and stated in the text. Unless otherwise stated, the 95% confidence interval derived from the curve fitting is given in brackets.

Biphasic normalized concentration-response curves were constructed and analyzed using GraphPad "Prism" version 5.0 according to the equation:

$$I = I_0 + (I_{max} - I_0)^{*}\text{Fraction1} / \left(1+10^{\left(\left(LogEC_{50}{}^{1-[\mathrm{A}]}\right)^{*n}\mathrm{H}^1\right)}\right) + (I_{max} - I_0)^{*}(1 - \text{Fraction1}) / \left(1+10^{\left(\left(LogEC_{50}{}^{2-[\mathrm{A}]}\right)^{*n}\mathrm{H}^2\right)}\right)$$

Where $I_{\max}$ is the response to the 30μM ACh, I_0 is the response to a maximal inhibitory concentration of ligand [A] and n_{H1} and n_{H2} are the two Hill slopes of the curve. When fitting the biphasic curves to ACh, we constrained n_{H1} and n_{H2} to 1. We also constrained the n_H to 1 when evaluating the monophasic ACh curve for comparison, as described in [28]. The R^2 value to describe the goodness of fit of the curve to the data is shown when comparing data to either biphasic or monophasic response curves. Where appropriate, biphasic and monophasic fits were compared with an F-test using the analysis software Prism. The p-value expressed in the test will be based on the null hypothesis that the curve is a monophasic fit. Where indicated in the text, statistical comparisons between groups with single values were compared with a one-way ANOVA and Tukey's post-hoc tests. If a biphasic curve was determined by the F-test, values are described with the 95% confidence interval derived from fitting the curve. Statistical comparisons for curves with different conditions or different ratios of RNA injected were compared with a two-way ANOVA for the response to each point. For all curves, the EC_{50} or IC_{50} values for individual curves are described with the 95% confidence interval as derived from fitting the curve.

3.0 Results

3.1 Activation of α9α10 nAChR by ACh and inhibition by Vc1.1 are best described by biphasic concentration response curves

A concentration response curve to ACh in Ca^{2+} free, 1.8mM Ba^{2+} solution was constructed to oocytes injected with equal concentrations of α9 and α10 subunit mRNA (Fig 1A). In the external buffer Ca^{2+} was replaced with Ba^{2+} to prevent activation of endogenous Ca^{2+}-activated chloride channels [29]. The resulting concentration-response curve preferred a biphasic activation curve fit compared to a monophasic curve fit (F-value of 3.37; $p<0.05$), with EC_{50} values for ACh of 11μM and 281μM, respectively (Fig 1B, Table 1).

We then constructed an inhibition curve to Vc1.1, where the peak responses to 30μM ACh in the presence of increasing concentrations of Vc1.1 were measured. Vc1.1 was pre-applied for 180s to ensure that equilibrium with the antagonist was reached. Using curve-fitting analysis, a monophasic and biphasic curve fits were performed to the appropriate Hill equation. Comparison of goodness of fit of the curves with an F-test indicated that the best curve fit was biphasic ($R^2_{(biphasic)} = 0.893$, $R^2_{(monophasic)} = 0.861$, $p < 0.01$), with IC_{50} values for Vc1.1 of 34nM and 10μM, respectively (Fig 1C, Table 1).

3.2 Change in receptor stoichiometry shifts the ACh-response curve from a biphasic to a monophasic curve

Concentration-response curves were constructed to ACh in Ca^{2+} free, 1.8mM Ba^{2+} solution for each ratio of RNA injected (Fig 2). A ratio of 1:10 α9:α10 mRNA yielded currents that were too small to allow an accurate measure of an inhibition curve up to 6 days post-injection (data not shown). In contrast concentration-response curves could be constructed when the ratios of RNA injected were 10:1 and 1:3 α9:α10. When injected with excess α10 (α9:α10; 1:3), the ACh-activation curve exhibited a monophasic shape with an EC_{50} value of 22μM (Fig 2A, Table 1). Interestingly, cells injected with excess α9 (α9:α10; 10:1) show a biphasic activation curve to ACh with EC_{50}s of 10μM and 537μM, respectively, corresponding to high and low ACh sensitivity sites (Fig 2B, Table 1). When this was compared with a monophasic curve for 10:1, the “best model F-test” preferred a biphasic over a monophasic curve with an F-value of 8.69 ($p < 0.05$). This is similar to the trend that was observed with a 1:1 injection ratio that preferred a biphasic curve fit, with EC_{50} values of 11μM and 281μM for high- and low-sensitivity ACh sites, respectively.

An F-test comparing ACh concentration response curves of 10:1 and 1:3 stoichiometries showed that the two curves were significantly different from each other (F-value of 3.43, $p < 0.05$). Best-fit EC_{50}, Hill-slope and maximum values of ACh response curve of 10:1 injection ratio, when compared to 1:1 injection ratio using Prism analysis, showed no significant difference with F-value of 0.64 ($p > 0.59$), suggesting that both the 1:1 and 10:1 injection ratios produce similar receptor populations. In contrast, the best-fit values of 1:3 injection ratio were significantly different to 1:1 injection ratio with F-value of 3.75 ($p < 0.05$).

3.3 The Vc1.1 inhibition curves are altered by varying the mRNA injection ratios of α9 and α10 subunits

To determine whether varying the subunit abundance alters the Vc1.1 inhibition curve to ACh, we injected α9:α10 mRNA corresponding to ratios of 10:1 and 1:3. Vc1.1 inhibited ACh (30μM) in a biphasic manner when oocytes were injected with a 10:1 mRNA ratio (F-value, 14.3; $p < 0.05$). The IC_{50} values for Vc1.1 were 34nM and 3.2μM, respectively (Fig 3A, Table 1). A two-way ANOVA comparing the response at each concentration, and F-test comparing best-fit values (IC_{50s}, Hill-slopes and fractions), showed that the response to Vc1.1 at oocytes injected with a 10:1 mRNA ratio was not significantly different to the 1:1 injection ratio (F-value, 1.06; $p > 0.05$). The fraction of current inhibited with a low-sensitivity to Vc1.1 is inferred from the graph to be 36%.

In contrast, Vc1.1 inhibited 30μM ACh-evoked currents in oocytes injected with a 1:3 ratio of α9:α10 RNA in a monophasic manner with an IC_{50} of 1.5μM (Fig 3B, Table 1). As the relative abundance of α10 subunits was increased in this ratio, a greater proportion of receptors containing the low-sensitivity Vc1.1 site were detected. A biphasic curve could not be fitted to the data, and a comparison by two-way ANOVA and best-value F-test using prism analysis showed that responses were significantly different to the responses with a 1:1 ratio ($p < 0.05$).

3.4 Vc1.1 inhibition at α9α10 nAChRs is insurmountable by ACh

To determine if Vc1.1 and ACh compete for the same binding site(s) on the α9α10 receptor, ACh concentration-response curves in the presence of varying concentrations of Vc1.1 were constructed for the 10:1 and 1:3 α9 and α10 mRNA injection ratios. If the ACh and Vc1.1 bind at identical sites, the inhibition by Vc1.1 should be reduced by high ACh concentrations that occupy the majority of binding sites, leading to parallel shifts and surmountable inhibition [30]. In cells injected with 10:1, α9: α10 mRNA, there appears to be a 35% reduction in the efficacy of ACh in the presence of Vc1.1. The EC_{50} values of the low sensitivity ACh site appeared to increase with increasing concentrations of the antagonist although this was not significant. In contrast, the inhibition appears insurmountable for the high-sensitivity ACh site, as there was a reduction in the maximal ACh current but no significant change to the EC_{50} (Fig 3C, Table 2; $p>0.05$). The observed shifts of ACh concentration response curves in the presence of increasing concentrations of Vc1.1 were not parallel; suggesting possible co-operative effects of Vc1.1 and/or ACh to the α9α10 receptor. An F-test comparing ACh response curves in presence of 100nM Vc1.1 and 1.5μM Vc1.1, showed that the two curves were significantly different from each other (F-value of 10.69; $P < 0.05$). These results are not consistent with a single non-competitive, or single competitive, binding mode for Vc1.1 but highlight the existence of multiple Vc1.1 binding sites some of which may be distinct from the ACh-binding site or alternatively different receptor stoichiometries are expressed and are inhibited differently by Vc1.1

When oocytes are injected with excess α10 compared to α9, (α9:α10; 1:3 mRNA ratio) the ACh curves in the presence of Vc1.1 (1.5μM and 3μM) were insurmountable, as the maximum ACh currents were significantly reduced compared to ACh alone ($p<0.01$; n=4-5). For 1.5μM Vc1.1 the EC_{50} for ACh was similar to EC_{50} of ACh in the, absence of blocker.

In the presence of 3μM Vc1.1 the maximum ACh current remained similar to that of the 1.5μM Vc1.1, but the EC_{50} value for ACh shifted to the right (Fig 3D, Table 2). The maximal ACh current in the presence of 30nM Vc1.1 was not significantly different to the maximal current produced by ACh alone ($p>0.05$; n=3; Student's t-test) which contrasted data using 1.5μM and 3μM Vc1.1 (Fig 3D insert).

The differences in the curves between the two mRNA injection ratios (10:1 versus 1:3) when Vc1.1 was co-applied with ACh suggest an additional binding site for Vc1.1 at receptors that have incorporated more α9 subunits. The additional binding is unlikely to be the channel pore as Vc1.1 showed voltage independent block for both stoichiometries (data not shown).

3.5 The biphasic inhibition curve is not a result of α9 homomeric and α9α10 heteromeric populations of receptors

It's been previously shown that α9 receptors can form homomeric receptors when expressed *in vitro*. One interpretation of a biphasic inhibition curve would be that the Vc1.1 has separate affinities for the α9 homomeric and α9α10 heteromeric receptors. To determine if the fraction of the current could be contributed by the α9 homomeric receptor, we injected α9 and α10 receptor mRNA alone and measured the peak currents elicited by 30μM ACh. In ND96 or Ca^{2+} free, 1.8mM Ba^{2+} solution, the peak response was never higher than 4 nA. However, this may be due to the presence of the divalent ions Ca^{2+}, Ba^{2+} and Mg^{2+} in the solutions as all have been shown to block α9 receptors [31]. When the external solution was changed to “low divalent” buffer, the peak current was significantly enhanced (Fig 4A). This is in agreement to the results obtained by Katz et al [31]. Irrespectively, the currents were still too small to accurately measure concentration response curves (<18 nA, n=13 for α9 homomeric receptors, c.f $55 \leq I \leq 448$ nA, n=7 for α9α10 receptors injected at the same concentration in Ca^{2+} free, 1.8mM Ba^{2+} solution) (Fig 4B). This is consistent with other studies [31] and demonstrates that α9 homomeric receptors make little or no contribution to the 30μM ACh-evoked current, eliminating these receptors as the cause of the biphasic inhibition curve. Injection of α10 mRNA alone did not result in ACh-evoked currents (data not shown), consistent with all the available literature [26]. To determine if the poly-adenylation within the oocyte was consistent between the two constructs, mRNA was transcribed from *Hind*III-cut DNA and poly-Adenylated *in vitro*. The inhibition of 30μM ACh by 1μM Vc1.1 applied to cells injected with a 1:1 α9:α10 ratio was similar for either transcription method ($I/I_{30\mu MACh}$=0.52±0.023 *Hind*III n=3, $I/I_{30\mu MACh}$=0.48±0.02 *Nhe*I, n=4, $p > 0.05$), and *Hind*III-cut DNA was used for subsequent experiments.

3.6 Effect of calcium on Vc1.1 inhibition at α9α10 nAChRs

Ca^{2+} is known to modulate the α9α10 nAChRs [32]. It is plausible that the different affinities and behavior of Vc1.1 in our experiments compared to the literature is a result of Ca^{2+} modulation. To test this, we measured the peak response of oocytes injected with equal concentrations of the α9 and α10 subunits to 1μM Vc1.1 and 30μM ACh, a concentration that elicits approximately 50 % of the current of 30μM ACh alone (Fig 1C). We performed this experiment in ND96 (1.8mM Ca^{2+}) and Ca^{2+} free, 1.8mM Ba^{2+} solution and found that in ND96 the normalised current was significantly smaller than in Ca^{2+} free, 1.8mM Ba^{2+} solution ($I/I_{30\mu MACh}$=0.275±0.035 ND96 n=9, $I/I_{30\mu MACh}$=0.500±0.015 Ca^{2+}-free n=7,

mean±s.e.m, $p < 0.05$ ANOVA), including in experiments which were wholly conducted on the same cell ($I/I_{30\mu MACh}$=0.256±0.02 ND96 n=3, $I/I_{30\mu MACh}$=0.520±0.02 Ca^{2+}-free n=3, mean±s.e.m, $p < 0.05$ ANOVA) (Fig 5). Furthermore, 30μM ACh elicited currents with 4-fold greater peak amplitudes in ND96 than in Ca^{2+} free, 1.8mM Ba^{2+} solution on the same cell (I_{ND96}/I_{Cafree}=4.0±0.7, n=4). When Ca^{2+} crosses the membrane of an oocyte, the changes in the intracellular Ca^{2+} concentrations activate endogenous Ca^{2+}-activated chloride channels that are also measured in the two-electrode voltage clamp configuration [33]. To determine if this effect was due to external Ca^{2+} concentrations, rather than changes in internal Ca^{2+} concentrations, we repeated the experiment with ND96 external solution but placed 11mM EGTA in the internal pipette solution to buffer the internal Ca^{2+} concentration (Fig 5B). Ethylene glycol tetraacetic acid (EGTA) has previously been shown to be effective in preventing the activation of the Ca^{2+} channels [34] and the introduction of the chelating agent by the recording pipette has previously been described by Khiroug et al, [35]. This method prevented stimulation of Ca^{2+}-activated chloride channels with lysophosphatidic acid (LPA) or naringin [36]. The inhibition was similar to the inhibition in Ca^{2+} free, 1.8mM Ba^{2+} solution, but significantly different to ND96 alone ($I/I_{30\mu MACh}$=0.49±0.037 EGTA n=5, $p < 0.05$ cf ND96, ANOVA). To ensure that the Ca^{2+}-chelation was complete, we applied repeat ACh concentrations to the oocyte and began the experiment when stable repeat recordings were measured, and continued to use ACh as an internal standard throughout the experiment.

We then chelated the intracellular Ca^{2+} concentrations with 1,2-**b**is(o-**a**mino**p**henoxy)ethane-N,N,N',N'-**t**etra**a**cetic acid (BAPTA), known to buffer the Ca^{2+} concentrations more quickly but with a higher affinity for zinc and a greater propensity to interact with membranes and phospholipids than EGTA [37, 38]. Again, the inhibition was similar to the inhibition in Ca^{2+} free, 1.8mM Ba^{2+} solution ($I/I_{30\mu MACh}$=0.46±0.06 BAPTA n=8, $p < 0.05$ cf ND96, ANOVA), and BAPTA injection prevented Ca^{2+}-channel activation by LPA. Furthermore, we repeated both the ACh-evoked concentration response and Vc1.1 inhibition curve in ND96 external solution with 11mM EGTA in the pipette solution. The concentration-response curve was not significantly different to Ca^{2+} free, 1.8mM Ba^{2+} solution (EC_{50}=45μM, n_H=0.6 n=4, $p>0.05$ ANOVA) and the inhibition curve was similarly biphasic ($p < 0.05$) with similar IC_{50} and Hill co-efficients to the inhibition curve in Ca^{2+} free, 1.8mM Ba^{2+} solution (Fig 4C-E) (IC_{50}=17nM and 2.14μM, n=4)(Table 1). We also measured the inhibition curve of Vc1.1 to 30μM ACh after injection of 0.5nmol BAPTA. Comparison of goodness of fit of the curves with R^2 values indicated that the curve fit was indeed biphasic ($p < 0.05$), with IC_{50} values of 19nM and 4.6μM (Table 1). In comparison, the inhibition curve in ND96 alone was monophasic (IC_{50} = 58nM, n_H = 0.72, $p > 0.05$) and a comparison with the curve in Ca^{2+} free, 1.8mM Ba^{2+} solution by two-way ANOVA indicated that responses to ACh are significantly different ($p < 0.05$) (Fig 5C-E; Table 1). In contrast, there is no significant difference between the responses of the EGTA or BAPTA treated oocytes and the oocytes in Ca^{2+} free, 1.8mM Ba^{2+} solution ($p > 0.05$).

These results demonstrate that changes in the intracellular Ca^{2+} concentration, as opposed to the extracellular concentration of Ca^{2+}, greatly affect Vc1.1 inhibition of α9α10 receptors. These data also demonstrate that in this system, the EGTA successfully removes the effect of

Ca^{2+}-activated chloride channels similar to BAPTA and replacement of extracellular Ca^{2+} with Ba^{2+}. The differences between reported Vc1.1 inhibition curves may also be affected by the divalent ion concentration in the external solution, in addition to Ca^{2+}-activated chloride channel stimulation.

To demonstrate that Vc1.1 did not directly affect the Ca^{2+}-activated chloride channel, we co-applied 1μM Vc1.1 and 1μM LPA to uninjected oocytes. Vc1.1 did not prevent chloride channel activation (data not shown).

3.7 RgIA and atropine do not differentiate between stoichiometries of α9α10 nAChRs

To determine whether the biphasic curve was a unique property of Vc1.1 inhibition, we constructed inhibition curves to RgIA and atropine against 30μM ACh-evoked currents in oocytes injected with a 10:1 ratio of α9:α10 RNA, with ND96 external solution and 11mM EGTA pipette solution (Fig 6). This ratio was chosen as the previous experiments indicated that it would contain two populations of receptors. Both inhibition curves were monophasic and contained IC_{50}'s of 23nM and 0.98μM, respectively, similar to previously reported values [15]. This suggests that the affinity of RgIA and atropine is similar for the various stoichiometries of α9α10 receptors.

4.0 Discussion

There is growing evidence that heteromeric nAChR subtypes exist in different stoichiometric forms, each with distinct functional properties that will contribute to synaptic regulation for nicotinic signaling in the mammalian brain. In the present study, we provide pharmacological evidence that α9α10 nAChRs can also form different receptor stoichiometries *in vitro* with varying sensitivities to ACh and the α-CTx, Vc1.1.

The presence of different stoichiometries for nAChR is not in itself novel. Receptors made up of α4 and β2 subunits can form two distinct stoichiometries, either the $(\alpha4)_2(\beta2)_3$ or $(\alpha4)_3(\beta2)_2$ stoichiometry. These stoichiometries are thought to be present *in vivo* [39, 40], with the $(\alpha4)_3(\beta2)_2$ nAChR being the more predominant (~70-80%) subtype in the brain [41]. These receptor stoichiometries differ in their sensitivities to agonists such as ACh, and have distinct desensitization kinetics, unitary conductance [42, 43], Ca^{2+} permeability [44], sensitivity to Zn^{2+} modulation [45] and chronic exposure to nicotine [42, 46, 47].

Recent studies detail a binding site for ACh at the α4-α4 in addition to the α4-β2 sites in α4β2 nAChRs. This α4-α4 interface is unique to the $(\alpha4)_3(\beta2)_2$ nAChR stoichiometry and shows differential agonist sensitivities [28]. We also have shown that antagonists such as methyllycaconitine (MLA) can be covalently trapped at the α4-α4 interface of the $(\alpha4)_3(\beta2)_2$ receptor form, highlighting an additional binding site for MLA at this interface [48]. Recently, studies identify that agonists binding to the α4-α4 interface may stimulate receptor desensitization [49]. Taken together, these studies indicate that interfaces, other than the traditional ACh binding sites located at the α4-β2 interface, contribute to the pharmacological effects of agonists and antagonists.

Stoichiometric forms of other nAChR subtypes such as the α3β4 nAChR also exist [50] but the physiological relevance of these is still unknown. Recently, it was demonstrated that the α-CTx, AuIB, prepared in two distinct conformational forms, ribbon versus globular bind with different affinities to different receptor stoichiometries of the α3β4 nAChR. Thus, it is plausible that α-CTxs can differentiate between different stoichiometries of nAChRs.

The stoichiometry of the α9α10 nAChR has previously been suggested to exist as the $(\alpha9)_2(\alpha10)_3$ stoichiometry [21]. This conclusion came from a careful study utilizing gain-of-function M2 α9 and α10 mutants but despite varying the mRNA ratio, this approach could not detect alternative receptor stoichiometries. In our study, we used ACh and the α-CTx, Vc1.1 to differentiate between receptor stoichiometries.

In oocytes injected with excess α9 mRNA, ACh exhibited a biphasic concentration response curve. In contrast, there was a shift from a biphasic to monophasic ACh concentration response curve when an excess of α10 mRNA is injected into the oocyte, with a loss of the ACh low sensitivity site. As homomeric α9 nAChRs were difficult to express and that the EC_{50} of ACh at α9 nAChRs is approximately 10μM [27] as compared to approximately 300μM for the heteromeric receptor (Table 1), the receptor populations observed are most likely due to different receptor stoichiometries of α9α10 and not contamination of α9 nAChRs. Therefore in analogy to the α4β2 and α3β4 nAChRs, we propose that the α9α10 nAChRs exist in at least two stoichiometric forms. We propose that the most likely stoichiometries are $(\alpha9)_3(\alpha10)_2$ and $(\alpha9)_2(\alpha10)_3$, although we cannot rule out the possibility of a $(\alpha9)_4(\alpha10)$ stoichiometry. We propose that ACh has an additional low sensitive binding site located at the α9-α9 interface, in addition to the computationally established α9-α10 binding site [22] that is common to both stoichiometries.

In addition, Vc1.1 displays a biphasic inhibition curve in the presence of ACh when receptors are formed with excess α9 mRNA. We propose that Vc1.1 is antagonizing the response of ACh at the $(\alpha9)_3(\alpha10)_2$ stoichiometry, most likely due to Vc1.1 binding to multiple sites on this receptor with variable binding sensitivities. Furthermore, there is an observed shift from biphasic to a monophasic inhibition curve when excess α10 mRNA is used, most likely due to a shift in stoichiometry from $(\alpha9)_3(\alpha10)_2$ to $(\alpha9)_2(\alpha10)_3$. Taken together, this data suggest the possibility of an additional high-sensitivity site for Vc1.1, most likely at the α9-α9 interface in the putative $(\alpha9)_3(\alpha10)_2$ stoichiometry. This is in addition to the known α10-α9 and the possible α9-α10 interface binding sites for Vc1.1 [22] that are common to both stoichiometries, that mediate the low-sensitivity Vc1.1 site. The additional binding is unlikely to be the channel pore as Vc1.1 showed voltage independent block (data not shown). In contrast, RgIA and atropine do not differentiate between stoichiometries of α9α10 nAChRs.

The concentration-response curves of ACh in the presence and absence of Vc1.1 also highlight the existence of additional binding sites for both ACh and Vc1.1 at the different α9α10 stoichiometries. The apparent insurmountable inhibition of the ACh concentration-response curves in receptors formed from excess α10 mRNA, that is the $(\alpha9)_2(\alpha10)_3$ form, indicates that Vc1.1 is either binding to two distinct sites, and/or that Vc1.1 is desensitizing

the receptor that occurs during the 180s pre-incubation of Vc1.1 prior to the co-application with ACh.

A much greater complexity of the ACh curves are observed when receptors are formed from an excess of α9 mRNA, proposed to be $(\alpha9)_3(\alpha10)_2$ nAChRs. These complex and dis-proportional (unparalleled) shift in ACh response curves are difficult to interpret and may be a combination of the following: co-operative effects between ACh and Vc1.1; an additional binding site for Vc1.1 and ACh located an α9-α9 interface; and/or differing arrangements of subunits to create different populations of receptors (e.g α9α9α9α9α10; α9α9α9α10α10 and α9α10α9α9α10). Like for what we observe for the $(\alpha9)_2(\alpha10)_3$ stoichiometry, there appears to be a reduction in the efficacy of ACh in the presence of Vc1.1. This may be due to an induced conformational change to the receptor that increases the probability of the receptor to be in a desensitized-like state, a phenomenon also observed by other nAChR antagonists [48]. Alternatively, Vc1.1 is binding at a site distinct from ACh and is unable to displace Vc1.1 at high concentrations. Finally, the concentrations of ACh required to displace Vc1.1 from one site may be higher than can be practically applied, and so appears as insurmountable inhibition.

This study contrasts previous studies that showed the receptor stoichiometry of α9α10 nAChR to be $(\alpha9)_2(\alpha10)_3$ [21] and also from studies that showed the antagonistic action of Vc1.1 on α9α10 receptors to be monophasic [16, 51, 52]. It is, however, in agreement with the [3H]epibatidine displacement binding studies that demonstrate a biphasic binding curve for Vc1.1 with a K_i of 2.3nM and 3.7μM [14], although the K_i values cannot be directly compared with IC_{50} values.

We infer that the observed variability in Vc1.1 inhibition between research groups is due to the use of Ca^{2+} in the buffer. Originally, experiments testing the potency of Vc1.1 on α9α10 nAChRs were performed with a fixed Ca^{2+} concentration (1.8mM), most likely to ensure recording conditions were as close to physiological conditions as possible. These conditions resulted in a monophasic Vc1.1 inhibition curve [16]. In this study, we investigated Ca^{2+}-dependence of Vc1.1 inhibition and determined that maintaining an intracellular concentration free of Ca^{2+} resulted in a biphasic curve. One explanation for the differing results is that the rise in intracellular Ca^{2+} concentration that occurs when ACh activates the α9α10 receptor leads to the opening of endogenous Ca^{2+}-activated chloride channels expressed in oocytes. At the holding potential used in these experiments, this would result in an inward current, thus increasing the signal above the actual activation of α9α10 receptors alone. This increase has been estimated to be as high as 10-fold [26], we measured a 4-fold increase in currents elicited by the EC_{50} ACh concentration, and may lead to an increase in the apparent sensitivity of Vc1.1 to α9α10 receptors. Alternatively it is also possible that at higher concentrations of Vc1.1, either the Ca^{2+}-activated chloride channels or another receptor is being non-specifically targeted. However, we demonstrate that Vc1.1 does not block these channels and that high concentrations of Vc1.1 are required to block α9α10 receptors composed of more α10 subunits. In addition, we demonstrate that the shape of the curve is altered from a biphasic to a monophasic curve when the effect of Ca^{2+} is not buffered in standard ND96. Therefore, as previously reported, and demonstrated here, the monophasic response to Vc1.1 may be due a significant increase in current flowing through

the Ca^{2+}-activated chloride channel compared to the current flowing through the α9α10 receptor [26]. This may lead to the chloride channel contributing the vast majority of the current that is recorded in ND96, masking the biphasic effect. It is also possible that different stoichiometries of the receptor have differing Ca^{2+} permeability, resulting in only one stoichiometry being effectively measured in the ND96 external solution in the absence of intracellular Ca^{2+} buffering. Thus it is recommended that experiments be performed either in Ca^{2+} free, 1.8mM Ba^{2+} solution or ND96 with the Ca^{2+} chelator.

In summary, we have shown that α9α10 nAChRs give rise to a biphasic activation curve for ACh, and a biphasic inhibition curve to Vc1.1 that is dependent on maintaining oocytes free of intracellular Ca^{2+}. This curve is altered to a monophasic curve when oocytes are injected with more α10 with respect to α9 RNA. By analogy to the α4β2 nAChRs, we propose that α9α10 nAChR exists in at least two distinct stoichiometries, possibly $(α9)_2(α10)_3$ and $(α9)_3(α10)_2$, with a high-sensitivity site for Vc1.1 at $(α9)_3(α10)_2$ and a low-sensitivity site that is common to both stoichiometries. Further studies are required to show whether these stoichiometries occur *in vivo*, whether they change in development, between different species or individuals and whether this will have consequences for drug therapies that target α9α10 nAChRs. Particularly, ligands that bind specifically to α9-α9 interface would be pharmacologically relevant as they target one stoichiometry without affecting the other. This is the first study showing the existence of an α9-α9 binding site that is unique to the $(α9)_3(α10)_2$ subtype that is proposed to be the high-sensitivity site for Vc1.1. This work adds to the growing evidence for the presence of different stoichiometries of nAChR subtypes.

Acknowledgements

MDM and MC acknowledge the support of Australian Research Council Discovery Grant DP0986469. JMM is supported by NIH Grants GM48677 and GM103801.

References

1. Betz H. Ligand-Gated Ion Channels in the Brain - the Amino-Acid Receptor Superfamily. Neuron. 1990; 5:383–92. [PubMed: 1698394]
2. Gotti C, Clementi F, Fornari A, Gaimarri A, Guiducci S, Manfredi I, et al. Structural and functional diversity of native brain neuronal nicotinic receptors. Biochem Pharmacol. 2009; 78:703–11. [PubMed: 19481063]
3. Unwin N. Refined structure of the nicotinic acetylcholine receptor at 4 angstrom resolution. J Mol Biol. 2005; 346:967–89. [PubMed: 15701510]
4. Miyazawa A, Fujiyoshi Y, Unwin N. Structure and gating mechanism of the acetylcholine receptor pore. Nature. 2003; 423:949–55. [PubMed: 12827192]
5. Elgoyhen AB, Katz E, Fuchs PA. The nicotinic receptor of cochlear hair cells: A possible pharmacotherapeutic target? Biochem Pharmacol. 2009; 78:712–9. [PubMed: 19481062]
6. Katz E, Elgoyhen ABN, Gomez-Casati ME, Knipper M, Vetter DE, Fuchs PA, et al. Developmental regulation of nicotinic synapses on cochlear inner hair cells. J Neurosci. 2004; 24:7814–20. [PubMed: 15356192]
7. Vetter DE, Katz E, Maison SF, Taranda J, Turcan S, Ballestero J, et al. The alpha 10 nicotinic acetylcholine receptor subunit is required for normal synaptic function and integrity of the olivocochlear system. Proc Natl Acad Sci USA. 2007; 104:20594–9. [PubMed: 18077337]
8. Elgoyhen AB, Katz E. The efferent medial olivocochlear-hair cell synapse. J Physiol. 2012; 106:47–56.

9. Peng HS, Ferris RL, Matthews T, Hiel H, Lopez-Albaitero A, Lustig LR. Characterization of the human nicotinic acetylcholine receptor subunit alpha (alpha) 9 (CHRNA9) and alpha (alpha) 10 (CHRNAIO) in lymphocytes. Life Sci. 2004; 76:263–80. [PubMed: 15531379]
10. Lustig LR, Peng H, Hiel H, Yamamoto T, Fuchs PA. Molecular cloning and mapping of the human nicotinic acetylcholine receptor alpha10 (CHRNA10). Genomics. 2001; 73:272–83. [PubMed: 11350119]
11. Kurzen H, Berger H, Jager C, Hartschuh W, Naher H, Gratchev A, et al. Phenotypical and molecular profiling of the extraneuronal cholinergic system of the skin. J Invest Dermatol. 2004; 123:937–49. [PubMed: 15482483]
12. Kumar P, Meizel S. Nicotinic acetylcholine receptor subunits and associated proteins in human sperm. J Biol Chem. 2005; 280:25928–35. [PubMed: 15894803]
13. Lips KS, Pfeil U, Kummer W. Coexpression of alpha 9 and alpha 10 nicotinic acetylcholine receptors in rat dorsal root ganglion neurons. Neurosci. 2002; 115:1–5.
14. Sandall DW, Satkunanathan N, Keays DA, Polidano MA, Liping X, Pham V, et al. A novel alpha-conotoxin identified by gene sequencing is active in suppressing the vascular response to selective stimulation of sensory nerves in vivo. Biochem. 2003; 42:6904–11. [PubMed: 12779345]
15. Ellison M, Feng ZP, Park AJ, Zhang X, Olivera BM, McIntosh JM, et al. alpha-RgIA, a novel conotoxin that blocks the alpha 9 alpha 10 nAChR: Structure and identification of key receptor-binding residues. J Mol Biol. 2008; 377:1216–27. [PubMed: 18295795]
16. Vincler M, Wittenauer S, Parker R, Ellison M, Olivera BM, McIntosh JM. Molecular mechanism for analgesia involving specific antagonism of alpha 9 alpha 10 nicotinic acetylcholine receptors. Proc Natl Acad Sci USA. 2006; 103:17880–4. [PubMed: 17101979]
17. Callaghan B, Haythornthwaite A, Berecki G, Clark RJ, Craik DJ, Adams DJ. Analgesic alpha-Conotoxins Vc1.1 and Rg1A Inhibit N-Type Calcium Channels in Rat Sensory Neurons via GABA(B) Receptor Activation. J Neurosci. 2008; 28:10943–51. [PubMed: 18945902]
18. Cuny H, de Faoite A, Huynh TG, Yasuda T, Berecki G, Adams DJ. gamma-Aminobutyric Acid Type B (GABA(B)) Receptor Expression Is Needed for Inhibition of N-type (Ca(v)2.2) Calcium Channels by Analgesic alpha-Conotoxins. J Biol Chem. 2012; 287:23948–57. [PubMed: 22613715]
19. McIntosh JM, Absalom N, Chebib M, Elgoyhen AB, Vincler M. Alpha9 nicotinic acetylcholine receptors and the treatment of pain. Biochem Pharmacol. 2009; 78:693–702. [PubMed: 19477168]
20. Callaghan BAD. Analgesic α-conotoxins Vc1.1 and RgIA inhibit N-type calcium channels in sensory neurons of α9 nicotinic receptor knockout mice. Channels (Austin). 2010; 4:51–4. [PubMed: 20368690]
21. Plazas PV, Katz E, Gomez-Casati ME, Bouzat C, Elgoyhen AB. Stoichiometry of the alpha 9 alpha 10 nicotinic cholinergic receptor. J Neurosci. 2005; 25:10905–12. [PubMed: 16306403]
22. Perez EG, Cassels BK, Zapata-Torres G. Molecular modeling of the alpha 9 alpha 10 nicotinic acetylcholine receptor subtype. Bioorg Med Chem Lett. 2009; 19:251–4. [PubMed: 19013796]
23. Azam L, McIntosh JM. Molecular basis for the differential sensitivity of rat and human alpha 9 alpha 10 nAChRs to alpha-conotoxin RgIA. J Neurochem. 2012; 122:1137–44. [PubMed: 22774872]
24. Yu RL, Kompella SN, Adams DJ, Craik DJ, Kaas Q. Determination of the alpha-Conotoxin Vc1.1 Binding Site on the alpha 9 alpha 10 Nicotinic Acetylcholine Receptor. J Med Chem. 2013; 56:3557–67. [PubMed: 23566299]
25. Verbitsky M, Rothlin CV, Katz E, Elgoyhen AB. Mixed nicotinic-muscarinic properties of the alpha9 nicotinic cholinergic receptor. Neuropharmacol. 2000; 39:2515–24.
26. Elgoyhen AB, Vetter DE, Katz E, Rothlin CV, Heinemann SF, Boulter J. alpha 10: A determinant of nicotinic cholinergic receptor function in mammalian vestibular and cochlear mechanosensory hair cells. Proc Natl Acad Sci USA. 2001; 98:3501–6. [PubMed: 11248107]
27. Elgoyhen AB, Johnson DS, Boulter J, Vetter DE, Heinemann S. Alpha-9 - an Acetylcholine-Receptor with Novel Pharmacological Properties Expressed in Rat Cochlear Hair-Cells. Cell. 1994; 79:705–15. [PubMed: 7954834]

28. Harpsoe K, Ahring PK, Christensen JK, Jensen ML, Peters D, Balle T. Unraveling the High- and Low-Sensitivity Agonist Responses of Nicotinic Acetylcholine Receptors. J Neurosci. 2011; 31:10759–66. [PubMed: 21795528]
29. Rothlin CV, Katz E, Verbitsky M, Elgoyhen AB. The alpha 9 nicotinic acetylcholine receptor shares pharmacological properties with type a gamma-aminobutyric acid, glycine, and type 3 serotonin receptors. Mol Pharmacol. 1999; 55:248–54. [PubMed: 9927615]
30. Wyllie DJ, Chen PE. Taking the time to study competitive antagonism. Br J Pharmacol. 2007; 150:541–51. [PubMed: 17245371]
31. Katz E, Verbitsky M, Rothlin CV, Vetter DE, Heinemann SF, Elgoyhen AB. High calcium permeability and calcium block of the alpha 9 nicotinic acetylcholine receptor. Hear Res. 2000; 141:117–28. [PubMed: 10713500]
32. Weisstaub N, Vetter DE, Elgoyhen AB, Katz E. The alpha 9 alpha 10 nicotinic acetylcholine receptor is permeable to and is modulated by divalent cations. Hear Res. 2002; 167:122–35. [PubMed: 12117536]
33. Barish ME. A Transient Calcium-Dependent Chloride Current in the Immature Xenopus Oocyte. J Physiol. 1983; 342:309–25. [PubMed: 6313909]
34. Yao Y, Tsien RY. Calcium current activated by depletion of calcium stores in Xenopus oocytes. J Gen Physiol. 1997; 109:703–15. [PubMed: 9222897]
35. Khiroug SS, Harkness PC, Lamb PW, Sudweeks SN, Khiroug L, Millar NS, et al. Rat nicotinic ACh receptor alpha 7 and beta 2 subunits co-assemble to form functional heteromeric nicotinic receptor channels. J Physiol. 2002; 540:425–34. [PubMed: 11956333]
36. Yow TT, Pera E, Absalom N, Heblinski M, Johnston GA, Hanrahan JR, et al. Naringin directly activates inwardly rectifying potassium channels at an overlapping binding site to tertiapin-Q. Br J Pharmacol. 2011; 163:1017–33. [PubMed: 21391982]
37. Rousset M, Cens T, Van Mau N, Charnet P. Ca2+-dependent interaction of BAPTA with phospholipids. FEBS Lett. 2004; 576:41–5. [PubMed: 15474007]
38. Aballay A, Sarrouf MN, Colombo MI, Stahl PD, Mayorga LS. Zn2+ depletion blocks endosome fusion. Biochemical Journal. 1995; 312:919–23. [PubMed: 8554539]
39. Marks MJ, Whiteaker P, Calcaterra J, Stitzel JA, Bullock AE, Grady SR, et al. Two pharmacologically distinct components of nicotinic receptor-mediated rubidium efflux in mouse brain require the beta 2 subunit. J Pharmacol Exp Ther. 1999; 289:1090–103. [PubMed: 10215692]
40. Gotti C, Moretti M, Meinerz NM, Clementi F, Gaimarri A, Collins AC, et al. Partial deletion of the nicotinic cholinergic receptor alpha 4 or beta 2 subunit genes changes the acetylcholine sensitivity of receptor-mediated 86Rb+ efflux in cortex and thalamus and alters relative expression of alpha 4 and beta 2 subunits. Mol Pharmacol. 2008; 73:1796–807. [PubMed: 18337473]
41. Shafaee N, Houng M, Truong A, Viseshakul N, Figl A, Sandhu S, et al. Pharmacological similarities between native brain and heterologously expressed alpha 4 beta 2 nicotinic receptors. Br J Pharmacol. 1999; 128:1291–9. [PubMed: 10578144]
42. Nelson ME, Kuryatov A, Choi CH, Zhou Y, Lindstrom J. Alternate stoichiometries of alpha4beta2 nicotinic acetylcholine receptors. Mol Pharmacol. 2003; 63:332–41. [PubMed: 12527804]
43. Moroni M, Zwart R, Sher E, Cassels BK, Bermudez I. alpha 4 beta 2 nicotinic receptors with high and low acetylcholine sensitivity: Pharmacology, stoichiometry, and sensitivity to long-term exposure to nicotine. Mol Pharmacol. 2006; 70:755–68. [PubMed: 16720757]
44. Tapia L, Kuryatov A, Lindstrom J. Ca2+ permeability of the (alpha 4)(3)(beta 2)(2) stoichiometry greatly exceeds that of (alpha 4)(2)(beta 2)(3) human acetylcholine receptors. Mol Pharmacol. 2007; 71:769–76. [PubMed: 17132685]
45. Moroni M, Vijayan R, Carbone A, Zwart R, Biggin PC, Bermudez I. Non agonist-binding subunit interfaces confer distinct functional signatures to the alternate stoichiometries of the alpha 4 beta 2 nicotinic receptor: An alpha 4-alpha 4 interface is required for Zn2+ potentiation. J Neurosci. 2008; 28:6884–94. [PubMed: 18596163]
46. Kuryatov A, Luo J, Cooper J, Lindstrom J. Nicotine acts as a pharmacological chaperone to up-regulate human alpha 4 beta 2 acetylcholine receptors. Mol Pharmacol. 2005; 68:1839–51. [PubMed: 16183856]

47. Carbone AL, Moroni M, Groot-Kormelink PJ, Bermudez I. Pentameric concatenated (alpha 4)(2) (beta 2)(3) and (alpha 4)(3)(beta 2)(2) nicotinic acetylcholine receptors: subunit arrangement determines functional expression. Br J Pharmacol. 2009; 156:970–81. [PubMed: 19366353]

48. Absalom NL, Quek G, Lewis TM, Qudah T, von Arenstorff I, Ambrus JI, et al. Covalent trapping of methyllycaconitine at the alpha4-alpha4 interface of the alpha4beta2 nicotinic acetylcholine receptor: antagonist binding site and mode of receptor inhibition revealed. J Biol Chem. 2013; 288:26521–32. [PubMed: 23893416]

49. Eaton JB, Lucero LM, Stratton H, Chang Y, Cooper JF, Lindstrom JM, et al. The unique alpha4(+)/(−)alpha4 agonist binding site in (alpha4)3(beta)2 subtype nicotinic acetylcholine receptors permits differential agonist desensitization pharmacology vs. the (alpha4)2(beta2)3 subtype. J Pharmacol Exp Ther. 2013

50. Grishin AA, Wang CI, Muttenthaler M, Alewood PF, Lewis RJ, Adams DJ. Alpha-conotoxin AuIB isomers exhibit distinct inhibitory mechanisms and differential sensitivity to stoichiometry of alpha3beta4 nicotinic acetylcholine receptors. J Biol Chem. 2010; 285:22254–63. [PubMed: 20466726]

51. Nevin ST, Clark RJ, Klimis H, Christie MJ, Craik DJ, Adams DJ. Are alpha 9 alpha 10 nicotinic acetylcholine receptors a pain target for alpha-conotoxins? Mol Pharmacol. 2007; 72:1406–10. [PubMed: 17804600]

52. Halai R, Clark RJ, Nevin ST, Jensen JE, Adams DJ, Craik DJ. Scanning Mutagenesis of alpha-Conotoxin Vc1.1 Reveals Residues Crucial for Activity at the alpha 9 alpha 10 Nicotinic Acetylcholine Receptor. J Biol Chem. 2009; 284:20275–84. [PubMed: 19447885]

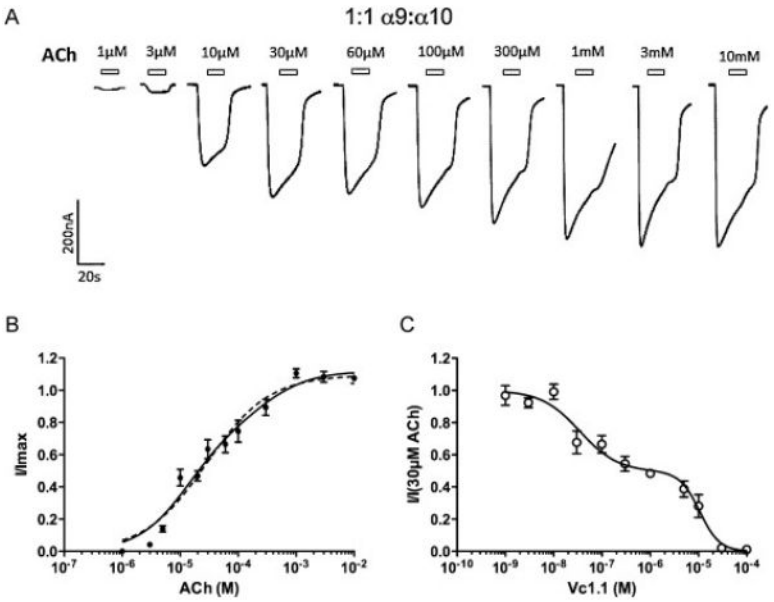

Figure 1.

A Representative traces of Ba^{2+} currents evoked by increasing concentrations of ACh in Ca^{2+} free, 1.8mM Ba^{2+} solution from a single oocyte expressing α9α10 receptors injected in a 1:1 subunit ratio. Open bars indicate ACh application. **B** Monophasic (dotted line) and biphasic (solid line) concentration-response curve to ACh (n=7). **C** Inhibition curve of 30 μM ACh-evoked by Vc1.1 (n=4).

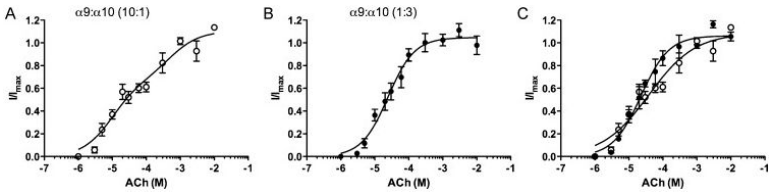

Figure 2.

A Concentration-response curve to ACh for oocytes expressing α9α10 injected in a 1:3 ratio in Ca^{2+} free, 1.8mM Ba^{2+} solution (n=4). Normalized data is shown as a solid line that fitted to a monophasic curve (●, solid line). **B** Concentration-response curve to ACh for oocytes expressing α9α10 injected in a 10:1 ratio in Ca^{2+} free, 1.8mM Ba^{2+} solution (n=4). A biphasic regression line is fitted through the normalized data shown as a solid line (○, solid line). **C** An overlay of α9α10 1:3 (●, solid line) and 10:1 (○, solid line) ratios from A and B.

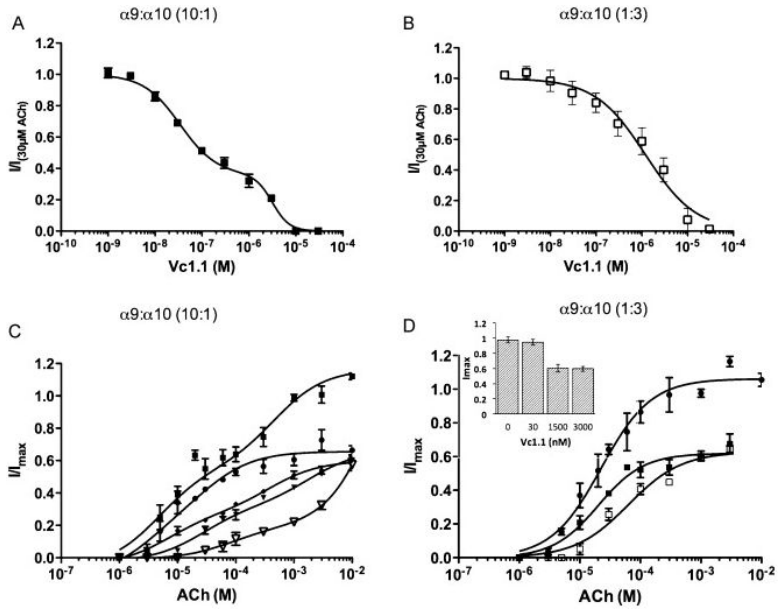

Figure 3.

A Inhibition curve of 30 μM ACh-evoked currents in Ca^{2+} free, 1.8mM Ba^{2+} solution by Vc1.1 in oocytes expressing α9α10 receptors injected in a 10:1 subunit ratio (n=4). Normalized response fitted to a biphasic regression line (■, solid line). **B** Inhibition curve of 30 μM ACh-evoked currents in Ca^{2+} free, 1.8mM Ba^{2+} solution by Vc1.1 in oocytes expressing α9α10 receptors injected in a 1:3 subunit ratio (n=4). Normalized response fitted to a monophasic regression line (□, solid line). **C.** ACh concentration response curve for α9α10 injected in a 10:1 ratio with varying concentrations of Vc1.1 - No Vc1.1 (■, solid line), 30nM Vc1.1 (●, solid line), 100nM Vc1.1 (◆, dashed line), 1.5μM Vc1.1 (▼, solid line), 3μM Vc1.1 (▽, solid line). **D** ACh concentration response curve for α9α10 injected in a 1:3 ratio in the presence of varying concentrations of Vc1.1 – No Vc1.1 (●, solid line), 1.5μM Vc1.1 (■, solid line), 3μM Vc1.1 (□, solid line). The inset compares the maximal ACh response in presence of various concentrations of Vc1.1 (0, 30, 1500 and 3000nM). Data are shown as mean ± s.e.m.

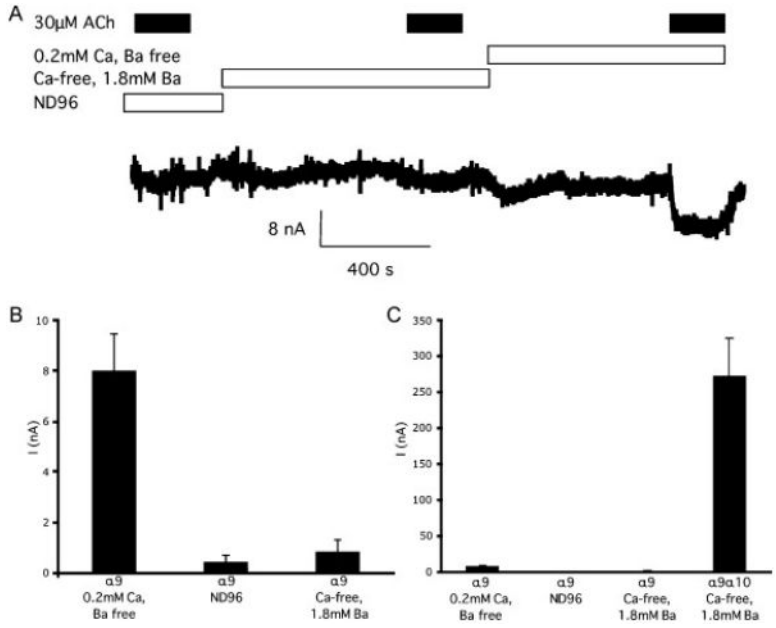

Figure 4.

A Representative trace of an ACh-evoked current in Ca^{2+} free, 1.8mM Ba^{2+} solution, ND96 and "low divalent" solutions from a single oocyte expressing homomeric α9 receptors. **B** Bar graph showing the mean response of α9 receptors in "low divalent" solutions, to 30 μM ACh and in ND96 and Ca^{2+} free, 1.8mM Ba^{2+} solution (n=8 measurable responses out of 15 oocytes in "low divalent" solutions). **C** Bar graph same as B except also showing the mean response of oocytes injected with α9 and α10 receptors at a 1:1 ratio in the same concentration as the α9 receptors in Ca^{2+} free, 1.8mM Ba^{2+} solution (n=11).

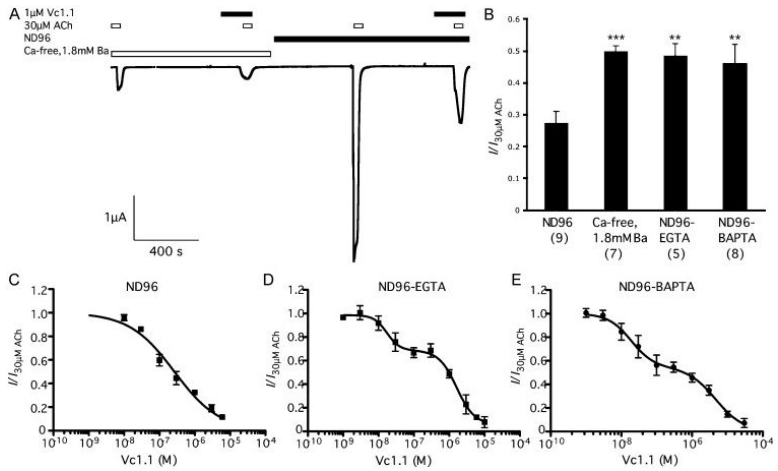

Figure 5.

A Representative trace from a single experiment superfused with Ca^{2+} free, 1.8mM Ba^{2+} solution (left) with response to 30 μM ACh and 30 μM ACh in the presence of 1 μM Vc1.1, then the same cell is superfused with ND96 and the response to 30μM ACh and 30 μM ACh in the presence of 1 μM Vc1.1. **B** Bar graph showing the response to 30 μM ACh and 1 μM Vc1.1 normalised to the response of 30 μM ACh for each cell. The responses in ND96, Ca^{2+} free, 1.8mM Ba^{2+} solution and ND96 with intracellular EGTA or BAPTA are shown as mean±s.e.m (n is shown in brackets, **p<0.01, ***p<0.001 one-way ANOVA, Tukey's post-hoc test). Note that the responses in ND96 and Ca^{2+} free, 1.8mM Ba^{2+} solution were derived from the same oocytes. **C-E** Inhibition curve of 30 μM ACh-evoked currents in ND96 solution by Vc1.1 in **(C)** ND96, **(D)** ND96 with intracellular EGTA and **(E)** ND96 after intracellular injection of BAPTA in oocytes expressing α9α10 receptors injected in a 1:1 subunit ratio (n≥4).

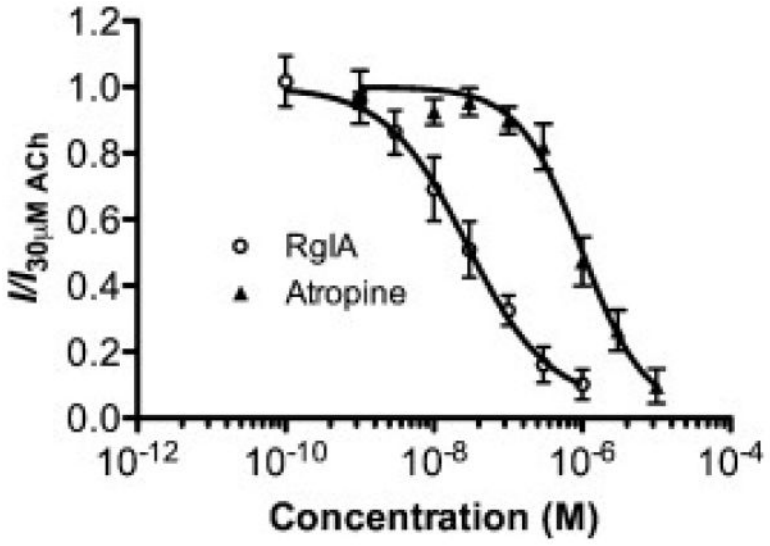

Figure 6.

Inhibition curve of 30 μM ACh-evoked currents by RgIA (○) and atropine (▲) in oocytes expressing α9α10 receptors injected in a 10:1 subunit ratio (n=3-5). Experiments were conducted in ND96 with 11mM EGTA in the recording pipettes. Data are shown as mean ± s.e.m.

Table 1

Ratio	ACh						Vc1.1					
α9 : α10	**EC_{50} (1) (μM)**	**EC_{50} (2) (μM)**	**Fraction high affinity**	**n_H (1)**	**n_H (2)**	**n**	**IC_{50} (1) (nM)**	**IC_{50} (2) (μM)**	**Fraction high affinity**	**n_H (1)**	**n_H (2)**	**n**
1:1	12 (4-32)	281 (43-1700)	0.56 (0.25-0.7)	1	1	7	34 (7-44)	11 (0.7-6.5)	0.50 (0.37-0.63)	1.1 (0-6)	2.4 (0.1-3)	5
1:3	22 (17-30)	nd	nd	1	nd	4	ND	1.6 (0.87-2.8)	nd	nd	nd	3
10:1	9.9 (4-21)	537 (79-3548)	0.60	1	1	4	34 (23-52)	3.2 (2.2-4.4)	0.64 (0.55-0.73)	1.1 (0.7-1.4)	2.1 (0.4-4.3)	4

Table 2

Values derived from curve fitting of ACh concentration response curve in the presence of varying concentrations of Vc1.1. 95% confidence intervals are given in brackets.

Ratio		ACh + Vcl.1			
α9 : α10	**Vcl.l (nM)**	**EC_{50} (1) (μM)**	**EC_{50} (2) (μM)**	**Fraction high affinity**	**n**
	0	22 (17-30)	nd	nd	4
1:3	1500	20 (14-29)	nd	nd	4
	3000	63 (42-95)	nd	nd	3
	0	9.9 (4-21)	537 (79-3548)	0.60	4
	30	18 (13-25)	nd	nd	3
10:1	100	6 (2-17)	390 (170-870)	0.49 (0.4 - 0.5)	4
	1500	27 (13-53)	1870 (770-4530)	~0.50	5
	3000	80 (22-285)	nd	0.10 (0 - 0.34)	4